



**HAL**  
open science

# Characterization of a new bio-based and biodegradable blends of poly(3-hydroxybutyrate-co-3-hydroxyvalerate) and poly(butylene-co-succinate-co-adipate)

Benjamin Le Delliou, Olivier Vitrac, Mickael Castro, Stephane Bruzaud,  
Sandra Domenek

## ► To cite this version:

Benjamin Le Delliou, Olivier Vitrac, Mickael Castro, Stephane Bruzaud, Sandra Domenek. Characterization of a new bio-based and biodegradable blends of poly(3-hydroxybutyrate-co-3-hydroxyvalerate) and poly(butylene-co-succinate-co-adipate). *Journal of Applied Polymer Science*, 2022, 139 (19), pp.52124. 10.1002/app.52124 . hal-03539633

**HAL Id: hal-03539633**

**<https://hal.science/hal-03539633>**

Submitted on 19 Apr 2022

**HAL** is a multi-disciplinary open access archive for the deposit and dissemination of scientific research documents, whether they are published or not. The documents may come from teaching and research institutions in France or abroad, or from public or private research centers.

L'archive ouverte pluridisciplinaire **HAL**, est destinée au dépôt et à la diffusion de documents scientifiques de niveau recherche, publiés ou non, émanant des établissements d'enseignement et de recherche français ou étrangers, des laboratoires publics ou privés.

# Characterization of a new bio-based and biodegradable blends of poly(3-hydroxybutyrate-co-3-hydroxyvalerate) and poly(butylene-co-succinate-co-adipate)

*Benjamin Le Delliou<sup>1</sup>, Olivier Vitrac<sup>1</sup>, Mickael Castro<sup>2</sup>, Stephane Bruzaud<sup>2</sup>, Sandra Domenek<sup>1,a</sup>*

<sup>1</sup>UMR 0782 SayFood Paris-Saclay Food and Bioproduct Engineering Research Unit, INRAE, AgroParisTech, Université Paris-Saclay, 91300, Massy France

<sup>2</sup> University Bretagne Sud, UMR CNRS 6027, IRDL, F- 56100 Lorient, France;

<sup>a</sup>Corresponding author: Sandra Domenek, 1 rue des Olympiades, 91300 Massy, France  
sandra.domenek@agroparistech.fr

## Abstract

Melt blending of poly(3-hydroxybutyrate-co-3-hydroxyvalerate) and poly(butylene-co-succinate-co-adipate) was investigated by means of batch mixing at different weight ratios (100:0, 70:30, 50:50, 30:70 and 0:100). PHBV and PBSA were immiscible. PBSA formed small nodules in PHBV, while PHBV formed large inclusions in PBSA. In 50/50 wt% blends, a co-continuous structure was obtained. The crystallization rate of PHBV and PBSA increased in the blends, most probably due to mutual nucleation, except at the later stages, where PHBV crystallization rates slowed down inside the nodules and in the co-continuous structure. The mechanical properties were successfully modeled with the EBM model, including parallel and serial resistances and show that the rigidity of the material can be modulated using PBSA. The elongation at break is however governed by PHBV. The blends featured brittle fracture even if PBSA was the continuous phase. The analysis of the stress at break showed that the fracture could be ascribed to debonding at the interfaces and the fracture behavior of PHBV.

**Reference:** Le Delliou B, Vitrac O, Castro M, Bruzaud S, Domenek S (2022) Characterization of a new bio-based and biodegradable blends of poly(3-hydroxybutyrate-co-3-hydroxyvalerate) and poly(butylene-co-succinate-co-adipate). J Appl Polym Sci 139 (19):52124.

doi:<https://doi.org/10.1002/app.52124>

## Introduction

Polymers are largely used in short-lived products, such as food packaging or single use containers because they are low-cost, light-weight, easy to process, flexible over an extensive range of temperatures. Their service life is thus much shorter than their total life time, which leads to persistent environmental pollution if collection and end-of-life of the materials are not managed adequately.<sup>1</sup> One means to prevent persistent pollution is to substitute commonly used polymers by biodegradable and compostable materials with satisfying performance.

Polyhydroxyalkanoates (PHAs) are biobased thermoplastic polyesters which are biodegradable even in marine environment, but they have poor mechanical performance and are difficult to process. They are synthesized as carbon and energy storage compounds by numerous microorganisms when macronutrients such as oxygen, nitrogen, or phosphorus are limited but a carbon source is still available in the culture medium.<sup>2</sup> Today, the main commercial polymers are short-chain-length PHAs, represented by poly(3-hydroxybutyrate) (PHB), and the copolymer poly(3-hydroxybutyrate-*co*-3-hydroxyvalerate) (PHBV).<sup>2,3</sup> Their glass transition temperature ( $T_g$ ) ranges between 0 and 5 °C. The isotacticity of PHBV results in stiff and brittle materials with an elongation at break below 5 % and a stress at break between 30 and 40 MPa.<sup>4</sup> PHBV has, moreover, a very narrow processing window and degrades rapidly upon melting. Its low shear viscosity and elastic melt strength impede its processing by extrusion-blowing.<sup>5</sup> To increase the material performance of PHBV, blending with other polymers was already proposed as a promising strategy. In the perspective of preserving the biodegradability of the mixture, binary blends were already studied with polylactic acid (PLA),<sup>6-8</sup> polybutylene adipate-*co*-terephthalate (PBAT),<sup>5,9</sup> polybutylene succinate (PBS).<sup>10</sup> An improved toughness and the possibility of tuning the mechanical properties were found for blends based with PLA, PHBV, and PBS.<sup>11</sup> Poly(butylene-*co*-succinate-*co*-adipate) (PBSA) is an alternative to PBS and could be used to develop polymer blends with increased ductility. While great attention has been focused on the characterization of PHBV in literature, reports on PBSA are rare. The elongation at break of PBSA can reach up to 400 %.<sup>12</sup> It is a biodegradable polymer that can be partially or fully biobased.<sup>13</sup> The higher elongation at break and its lower  $T_g$  (-45 °C) make PBSA superior to PBS. In addition, the lower crystallinity of PBSA compared to its counterpart PBS, results in accelerated biodegradation.<sup>14</sup> Polyester blends of PBSA and PLA were already studied at ambient temperature and relative humidity.<sup>15,16</sup> Authors reported on immiscibility between both constituents, formation of small nodules of PBSA in PLA, a reduction in tensile modulus from about 2.7 GPa (neat PLA) to 1 GPa (PLA/PBSA 50/50) and a moderate

improvement of the elongation at break, up to  $\epsilon=6.5$  % for PLA/PBSA 70/30.<sup>16</sup> The combination of the brittle material PHBV, and the highly ductile PBSA is potentially interesting for obtaining bio-based and biodegradable blends with improved processing and mechanical properties.

The present study presents a detailed rheological, morphological, thermal and mechanical characterization of PHBV/PBSA blends. The impact of the blend composition and structure on viscosity, crystallinity and tensile modulus was quantified and interpreted using known models, such as mixing rules, Avrami-Jeziorny analysis for non-isothermal crystallization and Equivalent Box Model (EBM) model for tensile strength of blends.

## **Experimental section**

### **2.1. Materials**

Commercial PHBV (reference PHI 002) containing 3 mol% of hydroxyvalerate (HV) – according to technical datasheet – and PBSA (reference PBE 001) were purchased from NaturePlast (France). Polymers were dried at 70 °C under vacuum for at least six hours before use.

### **2.2. Processing of PHBV and PBSA blends and sheets**

PHBV and PBSA were blended at molten state within an internal mixer (model Rheoscam, Scamex, France) at 190 °C at 90 rpm for 9 min. PHBV was first introduced in the mixing chamber for 6 min to allow its melting. PBSA pellets were subsequently introduced and mixed for additional 3 min. Blended materials were processed by thermo-compression molding at 180 °C and 150 bar (thermocompression press model 15 T, Scamex, France). Typical torque curves recorded during mixing are presented in the supporting information S1 and thermogravimetric analysis in S2. Pellets were molten for 3 min and then compressed in successive steps at 80 and 150 bar for 1 min each. Aluminum foils of 200  $\mu\text{m}$  were used to control the sample thickness. Five blend ratios PHBV/PBSA were produced with the weight percent ratios: 100/0, 70/30, 50/50, 30/70, 0/100 wt%.

## 2.3. Characterization methods

### 2.3.1. Thermal characterization

Thermal properties of blends were assessed by Differential Scanning Calorimetry, DSC, (DSC1, Mettler Toledo, Switzerland) according to two complementary temperature programs shown in **Figure 1**. All measurements were carried out under nitrogen atmosphere (flowrate 50 mL min<sup>-1</sup>) using 5 to 10 mg of material sealed in 40  $\mu$ L aluminum pans. Calibration was carried out with Indium and Zinc standards. All measurements were duplicated.

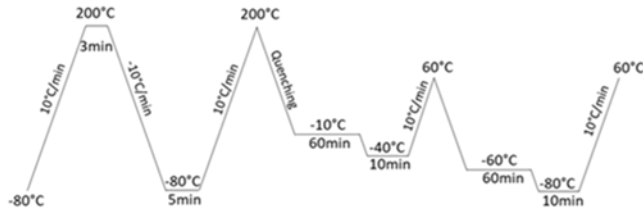
Program I (Figure 1) was used to measure melting and crystallization peaks and the glass transition temperature. Samples were heated from -80 °C to 200 °C at 10 °C min<sup>-1</sup> and held for 3 min at 200 °C, then cooled down to -80 °C at -10 °C min<sup>-1</sup> and held for 5 min at -80 °C, and subsequently heated to 200 °C at 10 °C min<sup>-1</sup>. The glass transition temperature ( $T_g$ ) was measured by quenching the sample from 200 °C to -10 °C for 60 min to physically age PHBV then cooling down to -40 °C for 10 min and heating to 60 °C at 10 °C min<sup>-1</sup>. Then physical aging of PBSA was carried out at -60 °C for 60 min, followed by cooling to -80 °C for 10 min, and heating to 60 °C at 10 °C min<sup>-1</sup>. The crystallinity of each polymer  $[\chi_i]_{i=PHBV,PBSA}$  was determined from the melting endotherm  $\Delta H_{m,i}$  as:

$$\chi_i = \frac{\Delta H_{m,i} - \Delta H_{cc,i}}{w_i \Delta H_{m,i}^0}, \quad (1)$$

where  $w_i$  is the weight content of the corresponding polymer,  $\Delta H_{cc,i}$  the cold crystallization enthalpy and  $\Delta H_{m,i}^0$  the melting enthalpy of a 100 % crystalline polymer with pure PHBV (146 J/g),<sup>17</sup> and PBSA (113.4 J/g).<sup>18</sup>

Program II (Figure 1) was used to analyze the non-isothermal crystallization of PHBV and PBSA. Samples were heated up to 190 °C at 10 °C/min, annealed for 3 min to erase thermal history and cooled down to -60 °C. Crystallization temperatures ( $T_c$ ) and exotherms ( $\Delta H_c$ ) were measured at cooling rates -5, -10, -20, -30, -40 and -50 °C min<sup>-1</sup>.

**Program I: Determination  $T_m$ ,  $T_c$  and  $T_g$**



**Program II : Non-isothermal crystallization kinetic**

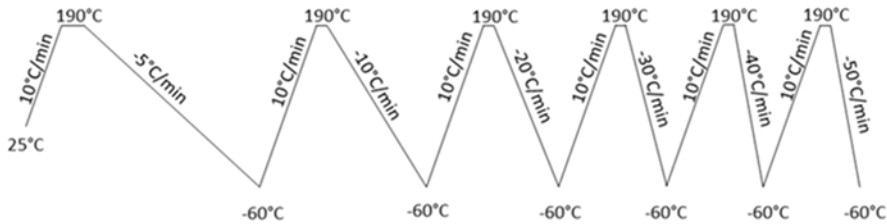


**Figure 1.** Schematic representation of the different DSC protocols

**2.3.2. Scanning electron microscopy**

The PHBV/PBSA blend morphology was observed thanks to Environmental Scanning Electronic Microscopy (model FEI Quanta 200, FEI Company, USA) with an accelerated voltage of 12 kV. Cryo-fractured samples were subjected to selective dissolution of the PBSA phase by tetrahydrofuran (THF) at room temperature for at least one hour. Selective dissolution of PBSA was carried out for ratios 70:30 and 50:50, because at higher PBSA content the sample integrity was not conserved. Samples were sputter-coated with a thin gold layer (model Sputter coater Emitech K550, Emitech, UK) and imaged from their cryo-fracture edges.

**2.3.3. Rheological properties**

Rheological properties were measured at molten state on 25 mm disk-shaped specimens placed in a stress-controlled rheometer (model MCR 302, Anton Paar, Graz, Austria) mounted with a parallel-plate geometry (gap 750-800  $\mu\text{m}$ ). Dynamic frequency sweep experiments were performed at 185 °C with frequency varying from 0.01 to 100 Hz in the linear viscoelastic region.

### 2.3.4. Mechanical properties

Tensile properties were measured using a texture analyzer (model TAHD, Stable Micro Systems, UK) equipped with pneumatic grips at a  $5 \text{ mm min}^{-1}$  crosshead speed. Dumbbell-shaped samples of type V ( $200 \mu\text{m}$ ) were cut from the compression-molded sheets. The sample thickness was averaged from five measurements with a caliper. At least five samples were tested for each blend composition.

### 2.3.5. Dynamic mechanical properties

Viscoelastic behavior of blends was characterized at 1 Hz and a stretch ratio of 0.1 % with a dynamic mechanical analyzer (model Tritec 2000 DMA, Triton Technology Ltd., UK). A temperature scan was performed from  $-60 \text{ }^\circ\text{C}$  to  $190 \text{ }^\circ\text{C}$  at a heating rate of  $2 \text{ }^\circ\text{C min}^{-1}$  on samples cut from thermocompression molded sheets (length = 10.25 mm, width = 5 mm).

## Results and discussion

### 3.1. Rheological properties

The viscoelastic properties of neat PHBV, PBSA, and PHBV/PBSA blends were analyzed with dynamic frequency sweep experiments from high to low frequencies, as shown in **Figure 2(a,b)**.

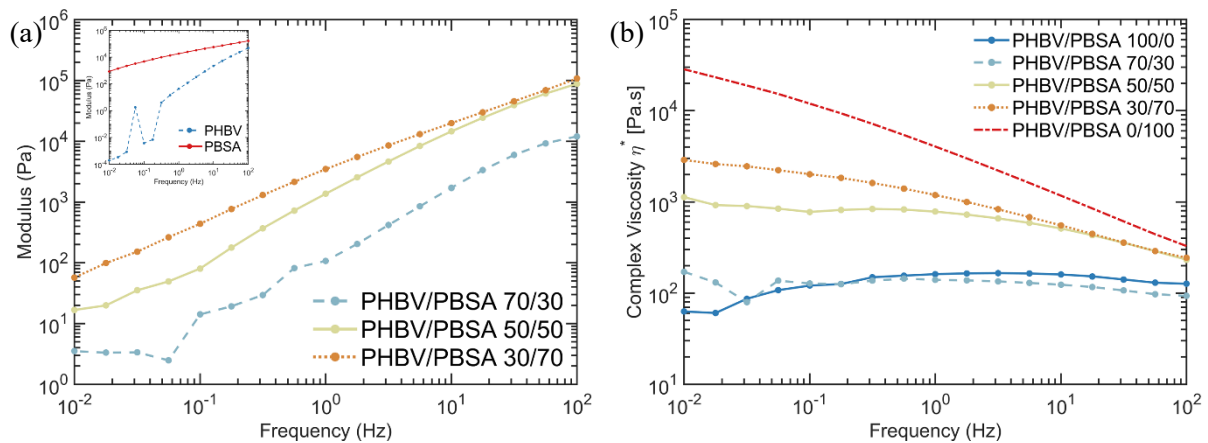


**Figure 2.** Mechanical spectrum of (a) storage modulus and (b) complex viscosity for neat PHBV, PBSA (insert in (a)), and PHBV/PBSA blends at  $185^\circ\text{C}$  after batch mixing. Data were recorded starting at high frequencies.

The insert in **Figure 2a** shows that PBSA featured typical terminal flow behavior with a terminal slope close to 2. PHBV showed a strong drop in modulus at 0.3 Hz caused by the thermal degradation of PHBV. For confirmation, an isothermal dynamic time sweep test of PHBV is available in the supplementary information S3. PHBV is known to degrade quickly above its melting temperature.<sup>19</sup> The storage modulus ( $G'$ ) of PHBV/PBSA blends was situated between the PHBV and PBSA values. It increased with rising PBSA content. The complex viscosity spectra (**Figure 2b**) evidenced that neat PHBV had Newtonian flow behavior in the observed frequency range while PBSA showed shear-thinning behavior. The change from PBSA dominated viscosity to PHBV dominated behavior was observed for blends with a concentration of PHBV equal to or higher than 50 wt%. This was indicative of an inversion of the continuous phase.

The flow of blends is characterized by the ratio of their shear viscosities ( $\eta$ ), the capillary number, and the ratio of viscous to surface forces.<sup>20</sup> The ratio of viscosity of one polymer with respect to the continuous phase,  $\lambda$ , predicts possible morphologies of two immiscible polymers. The critical capillary number gives the moment when shear forces overcome surface tension. Using the rheological data between 30 and 100 Hz,  $\eta_{PBSA}/\eta_{PHBV}$  (for PHBV as theoretical continuous phase) and  $\eta_{PHBV}/\eta_{PBSA}$  (for PBSA as theoretical continuous phase) were evaluated to 3.6 - 2.8 and 0.2 - 0.1, respectively. Large  $\lambda_{\eta_{PBSA}/PHBV}$  values are indicative for the high difficulty of dispersion of PBSA in PHBV as small droplets, whereas the formation of small droplets of PHBV in PBSA was very probable because of low  $\lambda_{\eta_{PHBV}/PBSA}$ . The complex viscosity of PHBV-PBSA mixtures ( $\eta_{mix}^*$ ) was calculated via a semi-logarithmic mixing rule:<sup>21</sup>

$$\log \eta_{mix}^* = w_{PBSA} \log \eta_{PBSA}^* + (1 - w_{PBSA}) \log \eta_{PHBV}^* \quad (2)$$

Predictions shown in **Figure 3** at different frequencies were in good agreement with experiments at PBSA concentration above 50 wt%, where small PHBV droplets were predicted. Phase separation was the likely cause of the deviation observed for 30 wt% PBSA, where large droplets were predicted.

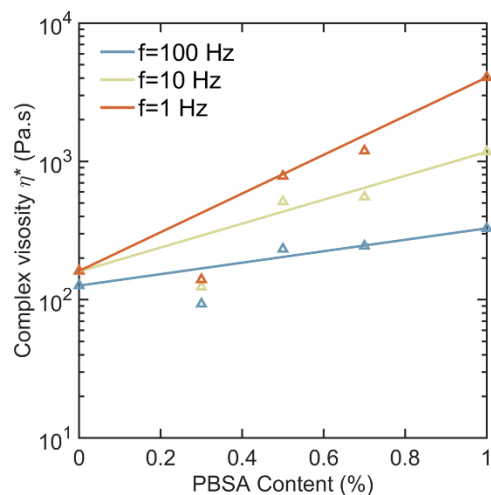


**Figure 3.** Complex viscosity of PHBV/PBSA blends as a function of PBSA content. Solid line represents the values calculated with the help of a semi-logarithmic mixing law.

### 3.2. Morphology of PHBV/PBSA blends

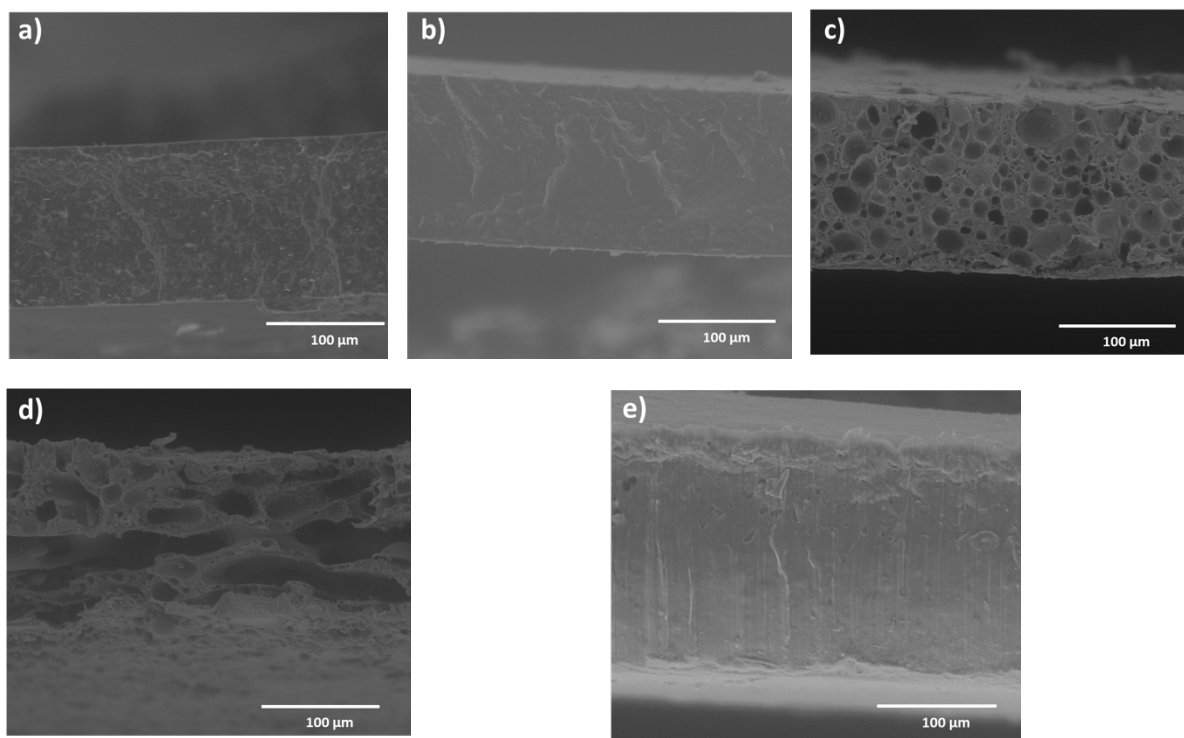


**Figure 4.** SEM images of cryo-fractured PHBV, PBSA and PHBV/PBSA blends: (a) neat PHBV, (b) neat PBSA, (c) PHBV/PBSA 70/30 after etching with THF at room temperature, (d) PHBV/PBSA 50/50 after etching with THF at room temperature, (e) PHBV/PBSA 30/70 (no etching).

The morphology of blends after melt-mixing and thermo-compression was observed on cryo-fractured samples by SEM (**Figure 4a-e**). Neat PBSA showed a smooth surface (Figure 4b), whereas neat PHBV presented a rugous surface (Figure 4a) with fractured crystallites and white items identified as inorganic fillers.<sup>7</sup> Phase separation was detected in PHBV/PBSA as expected from the rheological analysis. Figure 4c shows large PBSA droplets dispersed in PHBV for PHBV/PBSA 70/30 blend. For the PHBV/PBSA 50/50 blend, a co-continuous morphology was observed. Further increase in PBSA content led to a phase inversion, with small droplets of PHBV in PBSA as expected from viscosity ratios. The developed morphologies of PHBV/PBSA were typical of immiscible blends.

### 3.3. Thermal properties of PHBV/PBSA blends

#### 3.3.1. Melting behavior

Melting temperatures of neat PHBV and PBSA and of their blends were analyzed by DSC via protocol I (Figure 1). Two distinct melting points ( $T_m$ ) were identified at 174 °C and 86 °C for neat PHBV and PBSA, respectively. No significant change within the precision of the experiment in melting temperature was observed in binary blends. The tendency towards smaller  $T_m$  of PHBV might however suggest some compatibility. Details are reported in **Table 1**. Cold crystallization of PBSA was observed at  $T_{cc} \approx -5$  °C. Cold crystallization due to incomplete crystallization of the copolymer PBS<sub>59</sub>A<sub>41</sub> has been already described by Debuissy et al.<sup>22</sup>

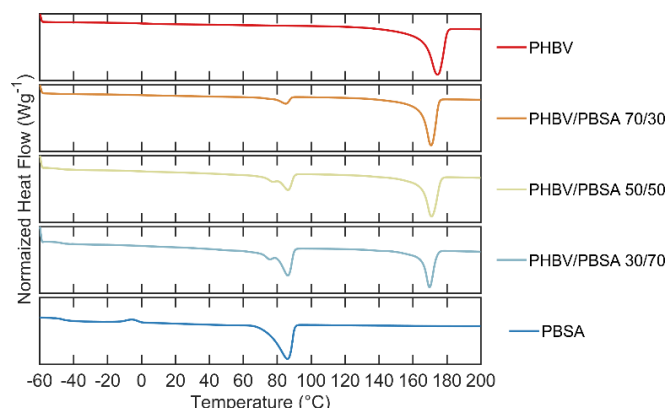


**Figure 5.** DSC curves of PHBV, PBSA and PHBV/PBSA blends recorded during the second heating scan following protocol I (exo up).

**Table 1.** Thermal properties of PHBV/PBSA blends measured by DSC during the cooling scan and the second heating scan.

PHBV/PBSA Samples	$T_m$ (°C)		$T_c$ (°C)		$\chi$ (%)		$T_g$ (°C)	
	PHBV	PBSA	PHBV	PBSA	PHBV	PBSA	PHBV	PBSA
100/0	171±3	n.d	122± 1	n.d	68±1	n.d	2.4±0.4	n.d
70/30	169±2	86±2	117±1	50±1	67±2	33±5	-1.5±0.1	-48.6±2.3
50/50	169±2	87±1	116±2	49±5	61±1	39±6	-3.1±0.8	-47.0 ±1.3
30/70	169±1	87±1	114±5	47±5	67±6	43±2	-3.3±0.3	-46.4±2
0/100	n.d	88±3	n.d	38±3	n.d	45±4 <sup>(a)</sup>	n.d	-45.9±1.6

<sup>(a)</sup> For calculation of the PBSA crystallinity degree, cold crystallization enthalpy was subtracted from the melting enthalpy.

### 3.3.2. Glass transition in the amorphous phase

Conventional heating scans are often not sensitive enough to reveal the glass transition of the amorphous phase of PHBV, because it accounts for a small quantity of the sample. The sensitivity problem is even higher in blends where the PHBV concentration is small. Therefore, a physical ageing treatment of PHBV or PBSA was applied to reveal the  $T_g$  using the enthalpy of relaxation peak. DSC thermograms are presented in **Figure 6a,b** and the quantified data are given in Table 1. Two separated  $T_g$  were identified in PHBV/PBSA blends, attributed to each of the polymers. The presence of two distinct  $T_g$  is consistent with the observation of a nodular blend structure due to immiscibility. In Table 1 a shift of the  $T_g$  of PHBV from 2 to -3 °C can be observed. This might indicate some level of compatibility between the polymers. The  $T_g$  of PBSA in the blends shifted also to lower temperatures. We suspect that thermal degradation of PBSA was the reason of that.

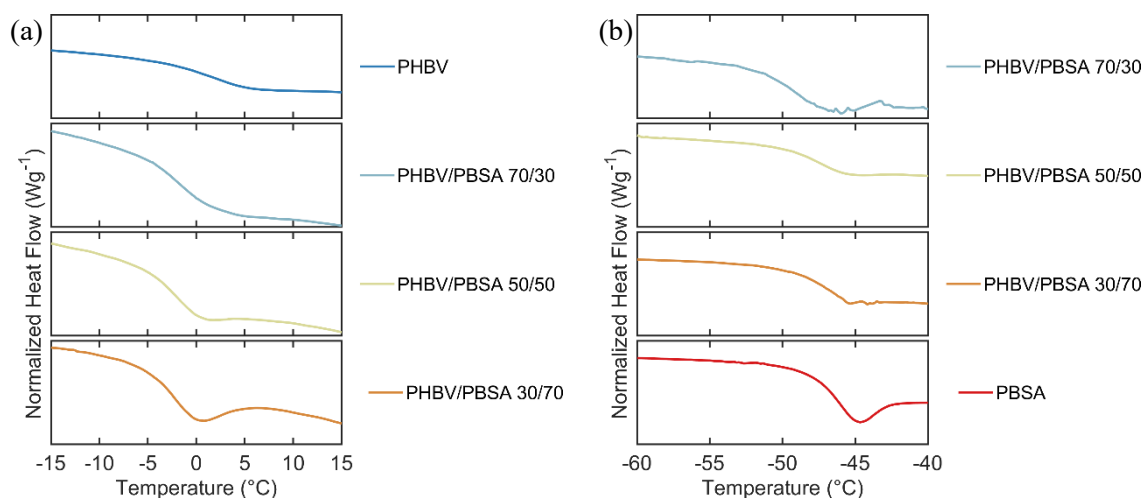


**Figure 6.** DSC curves of PHBV, PBSA and PHBV/PBSA blends. Figure 6a shows the  $T_g$  of PHBV after aging at  $-10\text{ }^\circ\text{C}$  and Figure 6b the  $T_g$  of PBSA after aging at  $-40\text{ }^\circ\text{C}$ .

### 3.3.3. Non isothermal crystallization kinetics of PHBV/PBSA blends

Crystallization kinetics of PHBV/PBSA blends were studied using non isothermal crystallization (program II, Figure 1). As shown in **Figure 7**, the crystallization peak temperature ( $T_c$ ) of PHBV in PHBV/PBSA blends shifted towards lower temperature, while an increase in the PBSA crystallization temperature with addition of PHBV was observed. All raw data are shown in the supplementary information S5. The quantification of the non-isothermal crystallization kinetics of the blends was carried out using the Avrami-Jeziorny method and Liu & Mo's model.<sup>23-26</sup> Both models are presented in the supplementary information S6.

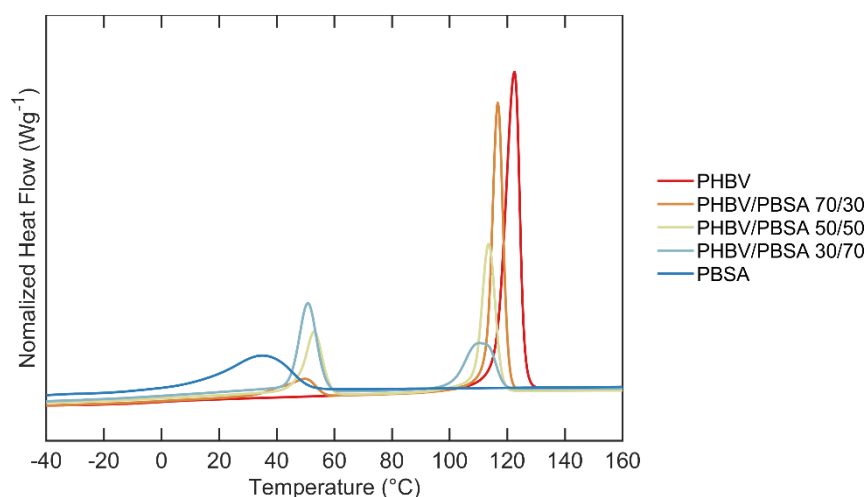


**Figure 7.** DSC thermogram of non-isothermal crystallization of PHBV, PBSA and PHBV/PBSA blends recorded during cooling at  $-10\text{ }^\circ\text{C min}^{-1}$  (protocol II).

The relative degree of crystallinity versus time for PHBV/PBSA blends showed a sigmoidal profile, indicative of the presence of secondary crystallization at higher crystallinity degrees (supplementary information S6). The linear part between 0.2 and 0.6 % relative crystallinity was used for the Avrami-Jeziorny analysis (supplementary information S6). The Avrami constants  $n_a$ ,  $k_a$ , and  $k_c$  are gathered in a synoptic table available in supplementary information S5. The normalized crystallization enthalpy  $H_c$ , crystallization peak temperature  $T_c$  and half time of crystallization  $t_{1/2}$  calculated with the help of the Avrami-Jeziorny constants are presented in **Table 2**. To help the observation, the data of Table 2 are repeated in graphical form in the supplementary information S6. No clear distinction could be made between the  $t_{1/2}$  (PHBV) and  $t_{1/2}$  (PHBV/PBSA 70/30). The  $t_{1/2}$  of the blends PHBV/PBSA 50/50 and 30/70 were smaller than the blank, except in case of the cooling rate 20 °C min<sup>-1</sup>. At this cooling rate, all  $t_{1/2}$  were very close and the PHBV blank value was smaller than the others. It seems that the PHBV crystallization is facilitated in the presence of interfaces with PBSA and in the smaller nodules. The change of the crystallization kinetics of PHBV in blends is much dependent on the nature of the second polymer. A slow-down of the isothermal PHBV crystallization kinetics was observed in PHBV/PCL blends,<sup>27</sup> and in PHBV/poly(styrene-co-acrylonitrile) blends.<sup>28</sup> In PHBV/poly(dicyclohexylitaconate) blends the PHBV crystallization kinetics seemed almost independent of the blend composition.<sup>29</sup> The acceleration of the PHBV crystallization kinetics was observed in PLA/PHBV blends using isothermal crystallization experiments at 125 °C when PHBV was in minority.<sup>30</sup> A small acceleration was also reported for isothermal crystallization of PHBV/PBS blends when the PHBV content decreased, which might be caused by a nucleating effect.<sup>31</sup> Because of the structural similarity of PBS and PBSA, we think that the small acceleration observed in the present work could be also linked to nucleation.

The acceleration of the PBSA crystallization kinetics in the blends was much more evident. The PBSA blank samples did not crystallize at a cooling rate higher than -30 °C min<sup>-1</sup>, but the PBSA phase crystallized in all blends. A tendency to smaller  $t_{1/2}$  (PBSA) was observed when the PHBV quantity of the blend increase. We conclude that PHBV acted as a nucleating agent for PBSA.

**Table 2.** Crystallization enthalpy normalized by the polymer content ( $H_c$ ), crystallization temperature ( $T_c$ ) and half time of crystallization ( $t_{1/2}$ ) calculated from the Avrami–Jeziorny parameters during non-isothermal crystallization of PHBV, PBSA and PHBV/PBSA blends.

Samples	Cooling rate (°C min <sup>-1</sup> )	PHBV			PBSA		
		$H_c$ (J g <sup>-1</sup> )	$T_c$ (°C)	$t_{1/2}$ (min)	$H_c$ (J g <sup>-1</sup> )	$T_c$ (°C)	$t_{1/2}$ (min)
PHBV	5	95	127.7	1.18			
	10	91	123.8	0.93			
	20	86	119.2	0.83			
	30	82	114.5	0.84			
	40	91	114.2	0.83			
	50	86	111.2	0.88			
PBSA	5				52	38.2	1.16
	10				49	29.3	0.94
	20				22	19.8	0.80
	30				4	n.d.	n.d.
	40				no crystallization		
	50				no crystallization		
PHBV/PBSA 70/30	5	97	123	1.03	42	58.9	0.96
	10	93	118.8	0.90	42	54	0.85
	20	88	113.9	0.87	42	48.6	0.80
	30	80	110.5	0.85	55	45.3	0.78
	40	79	108.5	0.85	28	39.7	0.77
	50	82	105.3	0.84	22	28.7	0.77
PHBV/PBSA 50/50	5	72	120.9	1.09	48	59	0.99
	10	93	116.4	0.90	48	54.4	0.86
	20	80	106.9	0.86	53	43.9	0.81
	30	89	111.5	0.80	46	48.7	0.80
	40	81	104.4	0.80	35	38.4	0.79
	50	87	101.2	0.82	28	26.2	0.79
PHBV/PBSA 30/70	5	82	120.1	1.06	56	55.5	1.03
	10	86	115.6	0.86	56	49.9	0.88
	20	82	110	0.84	67	43	0.83
	30	72	104.6	0.77	60	34	0.82
	40	77	101.4	0.78	39	26.5	0.80
	50	87	98.4	0.77	35	11.3	0.80

n.d. not determined

To go further in the kinetic analysis of the present study, the data were investigated with the model developed by Liu et al. 1997.<sup>23</sup> This model is characterized by two parameters,  $F(T)$  and  $m$  (ratio of Avrami and Ozawa exponents).  $F(T)$  represents the difficulty of the crystallization process, because it denotes the required cooling rate to achieve a given degree of crystallinity. The analysis of the experimental data is shown in the supplementary information S6. Both parameters,  $m$  and  $F(T)$  were obtained from the slope and the intercept of the as-defined linear

portion of  $\log \alpha$  versus  $\log t$  respectively. The results are gathered in **Table 3** and show that for both polymer phases,  $F(T)$  increased with increase of relative degree of crystallinity. This behavior is generally observed because the crystallization slows down at high crystallinity degrees. The comparison of the  $F(T)$  data of the blends shows that at the same level of crystallinity, the crystallization kinetics of the PHBV phase was sensitive to the blend morphology. The PHBV crystallization in blends was facilitated at the lower degrees of crystallinity, which is indicative of nucleation of PHBV by PBSA. At 20 % of crystallinity all  $F(T)$  values were decreased. At higher crystallinity degrees, the  $F(T)$  values of the PHBV/PBSA 50/50 and PHBV/PBSA 30/70 blends increased with respect to the blank value. The presence of PBSA in the co-continuous structure and, even more, the constraining of PHBV in small nodules hindered PHBV crystallization in its later stages. This was not true, if PBSA was dispersed as large nodules in the PHBV matrix. Here the crystallization was facilitated over the whole range of crystallinity degrees. All  $F(T)$  values of PBSA in blends were lower than the blank. Introduction of PHBV in PBSA facilitated the crystallization process notwithstanding the morphology. Nucleation might be the reason of that.<sup>32</sup>

**Table 3.** Liu parameters during non-isothermal crystallization of PHBV, PBSA and PHBV/PBSA blends.

Samples	$\chi(t)$ (%)	PHBV			PBSA		
		$m$	$F(T)$	$R^2$	$m$	$F(T)$	$R^2$
PHBV	20	0.92	10.11	0.97			
	40	0.97	12.87	0.97			
	60	1.04	15.88	0.98			
	80	1.01	22.61	0.97			
PBSA	20				1.02	14.39	0.92
	40				1.1	27.51	0.92
	60				1.18	43.78	0.91
	80				1.21	63.79	0.91
PHBV/PBSA 70/30	20	1.26	6.2	0.99	1.34	4.72	0.99
	40	1.31	8.56	1	1.45	9.67	0.99
	60	1.44	11.12	0.99	1.51	14.96	0.99
	80	1.51	20.21	1	1.48	23.65	0.99

PHBV/PBSA 50/50	20	1.17	8.61	0.99	1.4	5.26	0.99
	40	1.26	12.42	0.99	1.53	10.25	0.99
	60	1.44	18.48	1	1.6	15.77	0.98
	80	1.49	34.64	0.99	1.59	26.25	0.98
PHBV/PBSA 30/70	20	1.13	7.7	0.93	1.46	6.86	0.99
	40	1.12	13.61	0.9	1.63	13.45	1
	60	1.1	20.59	0.85	1.68	20.43	0.99
	80	1.1	29.73	0.83	1.65	32.99	0.99

### 3.4. Mechanical properties of PHBV/PBSA blends

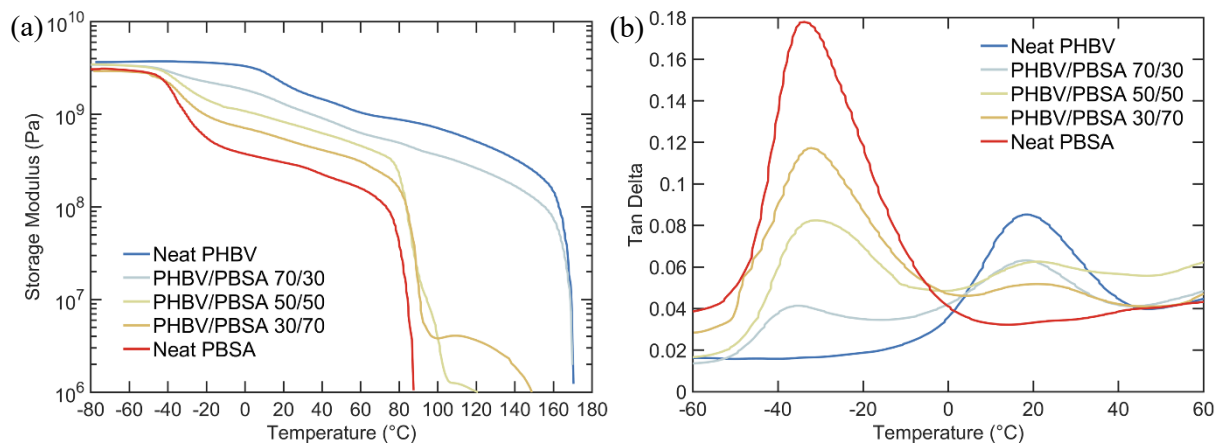


**Figure 8.** Evolution of (a) the elastic modulus and (b)  $\tan \delta$  as function of temperature for PHBV, PBSA and PHBV/PBSA blends.

**Figure 8a** shows the evolution of the elastic modulus ( $E'$ ) as function of temperature ranging from -60 °C to 180 °C. PHBV featured as expected higher storage modulus values over the whole temperature range than PBSA. The addition of PHBV to PBSA increased the height of the rubbery plateau modulus. It had only a moderate impact on the increase of the flow temperature of PBSA. Even in the co-continuous blend, the material flowed below 100 °C. In case of PHBV being the continuous phase, the decrease of the rubbery moduli of the nodular blends with respect to PHBV was observed without change in flow behavior. **Table 4** highlights  $E'$  values at relevant service temperatures, i.e. at room temperature (20 °C) and in freezer conditions (-20 °C). **Figure 8b** shows the evolution of  $\tan \delta$  as a function of temperature ranging from -60 °C to 60 °C. The peak of  $\tan \delta$  can be attributed to the dynamic glass transition. The

dynamic glass transition temperature  $T_{\alpha}$  was determined at the maximum value of the peak ( $T_{\alpha}$  values are available in in supplementary information S7). Two distinct  $T_{\alpha}$  were identified which is consistent with DSC data and shows the immiscibility of PHBV and PBSA.

**Table 4.** Determination of storage modulus  $E'$  and mechanical properties of PHBV/PBSA blends obtained from DMA and tensile test measurements.

PHBV/PBSA samples	$E'$ (MPa) from DMA		Tensile properties		
	-20 °C	20 °C	Young modulus <sup>(a)</sup> (MPa)	Stress at yield (MPa)	Elongation at break (%)
100/0	3625	2153	3485±63	22±2.0	0.98±0.1
70/30	2247	1297	2227±108	19±2.5	1.48±0.4
50/50	1438	829	1360±125	12±1.9	1.48±0.2
30/70	966	543	833±147	12±1.6	3.10±0.8
0/100	553	303	332±8	15±1.4	134.8±48

<sup>(a)</sup>experiments carried out without extensometer.

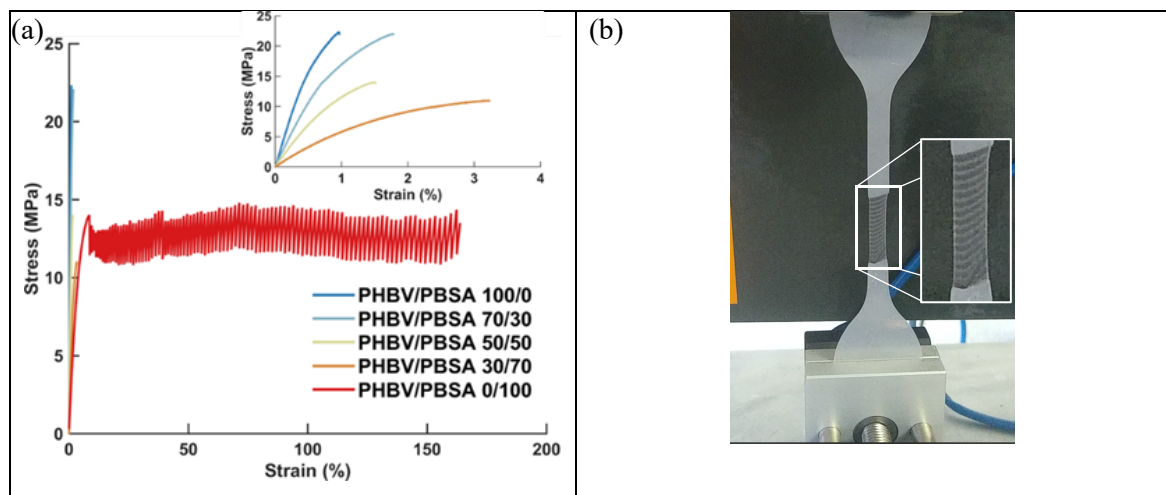


**Figure 9.** (a) Typical stress-strain curves of tensile test of PHBV, PBSA and PHBV/PBSA blends, (b) stress-oscillation of PBSA samples during tensile testing.

The mechanical properties of the PHBV-based blends were assessed with tensile tests. Typical stress-strain curves are shown in **Figure 9a**. Typical fragile behavior was observed for neat PHBV characterized by a low elongation at break. It has already been discussed by several

authors that the brittle behavior of PHBV can be caused by i) the cold crystallization of the amorphous phase at ambient temperature, ii) glass transition temperature close to room temperature, and iii) radial or circumferential cracks potentially contained in spherulites of PHBV with low content of 3HV.<sup>33,34</sup> The existence of these cracks is supposed to be caused by the difference in the thermal expansion coefficients of the material along the radius and the circumference of crystallites, which generates drastic internal stresses.<sup>2</sup>

PBSA featured ductile behavior with a high elongation at break. Stress-oscillation of pure PBSA was observed. The occurrence of stress-oscillation was reported for PBS as a consequence of alternating regions of highly oriented crystalline zones and micro-cavities due to crazing and voiding.<sup>35,36</sup> The phenomenon generated alternating transparent/opaque bands as shown in **Figure 9b**. A video of the phenomenon is available in supplementary information S8. **Table 4** reports the tensile properties of PHBV, PBSA and its blends. The apparent Young modulus was in accordance with the  $E'$  values at room temperature obtained by DMA. The increase of the PBSA content lowered the stress at break. The obtained elongation at break of the formulated blends was still small, though. Even when the ductile polymer PBSA was the continuous phase, the samples broke at only 3 % elongation. Apparently, although there might be some interfacial compatibility between PBSA and PHBV, an efficient stress transfer between both phases could not be achieved. The evolution of the elastic modulus with PBSA content is shown in **Figure 10a**. To understand the result, the data were modelled with using parallel (Reuss model) or serial resistances (Voigt model):

$$E^n = \phi_1 E_1^n + \phi_2 E_2^n, \quad (2)$$

Where  $E_1$  and  $E_2$  are the elastic modulus of phase 1 and 2,  $\Phi_1$  and  $\Phi_2$  the volume fraction of phase 1 and phase 2, and exponent  $n$  characterizes the type of model with  $n=1$  (parallel or Reuss model) or  $n=-1$  (Series or Voigt model). To account for a mixed behavior including parallel and serial resistances, the Equivalent Box Model (EBM)<sup>37</sup> was used. It is detailed in supplementary information S9. Based on the percolation theory, critical volume fractions were set to  $v_{1cr} = v_{2cr} = 0.16$ .<sup>38</sup> The resulting tensile modulus of two components blend ( $E_b$ ) is given as the sum  $E_p v_p + E_s v_s$ :<sup>37</sup>

$$E_b = E_1 v_{1p} + E_2 v_{2p} + v_s^2 / \left( \frac{v_{1s}}{E_1} + \frac{v_{2s}}{E_2} \right), \quad (3)$$

where  $E_1$  and  $E_2$  are the Young moduli of phases 1 and 2 and  $v_{i,p}$  and  $v_{i,s}$  are the total volume fractions of the parallel branch and series branch, respectively. The prediction of strength can be modeled as follows:<sup>39</sup>

$$S_b = S_1 v_{1p} + S_2 v_{2p} + AS_2 v_s, \quad (4)$$

where  $S_1 > S_2$  and  $S_1$  and  $S_2$  are the strength of phase 1 and 2, respectively.  $A$  corresponds to the level of interfacial bonding.

The comparison of the experimental results with the different models (**Figure 10a**) shows that the evolution of the Young modulus ( $E$ ) with increasing PBSA content in the blends was fairly well captured by the EBM model using the universal parameters. This observation further confirmed the immiscibility between both components. A similar observation was made on PHBV/PBS blends.<sup>10</sup> **Figure 10b** shows the modeling of the stress at yield of PHBV/PBSA blends. EBM is a predictive model, in that it indicates if the interfacial adhesion is strong ( $A=1$ ) or weak ( $A=0$ ). The results showed that a low adhesion factor ( $A$ ) needs to be assumed to describe the behavior of the blends at high PBSA content. The strain at break was at any composition lower than the strain at break of the stronger polymer, PHBV, which shows that the materials fractured by debonding at the interface.

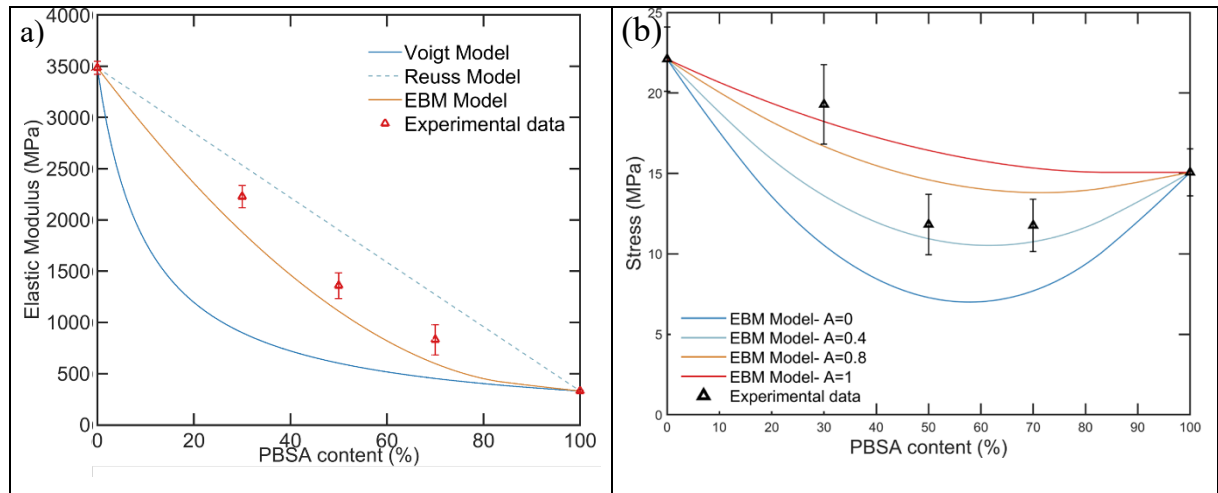


**Figure 10.** (a) Modeling of the elastic modulus from tensile testing of PHBV/PBSA blends depending on PBSA content using the Voigt, Reuss, and EBM model, (b) evolution of the tensile stress of PHBV/PBSA blends with representation of EBM model at different levels of interfacial adhesion ( $A$ ).

### 3.5. Conclusion

This study presents a detailed investigation of thermo-mechanical and rheological properties of PHBV/PBSA blends prepared by batch mixing. PHBV and PBSA were immiscible. As predicted by the viscosity ratio between the polymers and confirmed by SEM observation, PBSA formed small nodules in PHBV, while PHBV formed large inclusions in PBSA. A co-continuous blend morphology was observed in 50/50 PHBV/PBSA blends. The investigation of the crystallization kinetics showed that the crystallization rate of PHBV and PBSA increased

in the blends, most probably due to mutual nucleation. However, the crystallization rates observed at high PHBV crystallinity degree were slowed down when PHBV was dispersed in small nodules in PBSA or blends had co-continuous structure. The mechanical properties were successfully modeled with the EBM model, including parallel and serial resistances and showed that the rigidity of the material could be modulated using PBSA. The elongation at break was however governed by PHBV. Brittle fracture happened even in case PBSA was the continuous phase, in accordance with a model of serial resistances. The analysis of the adhesion factor showed that there was most likely debonding at the interfaces. In conclusion, PHBV/PBSA blends have improved melt viscosity and accelerated crystallization kinetics, but for successful improving mechanical properties supplementary compatibilizers will be necessary.

### Supporting Information

Supporting Information is available from the Wiley Online Library or from the author.

### Acknowledgements

The authors acknowledge financial support from the company McCain Alimentaire S.A.S and from ANRT (French National Association for Research and Technology via the CIFRE agreement n°2017/1574 attributed to Benjamin Le Delliou. The authors greatly thank Pierre Gondé for his technical support.

*Pack. Technol. Sci.*

### References

1. K. Verghese, H. Lewis, S. Lockrey, H. Williams, *Pack. Technol. Sci.* **2015**, *28*, 603, DOI: 10.1002/pts.2127.
2. B. Laycock, P. Halley, S. Pratt, A. Werker, P. Lant, *Prog. Polym. Sci.* **2014**, *39*, 397, <http://dx.doi.org/10.1016/j.progpolymsci.2013.06.008>.
3. M. Deroiné, A. Le Duigou, Y.-M. Corre, P.-Y. Le Gac, P. Davies, G. César, S. Bruzaud, *Polym. Test.* **2014**, *39*, 70, <https://doi.org/10.1016/j.polymertesting.2014.07.018>.
4. A. Anjum, M. Zuber, K. M. Zia, A. Noreen, M. N. Anjum, S. Tabasum, *Int. J. Biol. Macromol.* **2016**, *89*, 161.
5. M. Cunha, B. Fernandes, J. A. Covas, A. A. Vicente, L. Hilliou, *J. Appl. Polym. Sci.* **2015**, *133*, DOI: 10.1002/app.42165.
6. M. Boufarguine, A. Guinault, G. Miquelard-Garnier, C. Sollogoub, *Macromol. Mat. Eng.* **2013**, *298*, 1065, DOI: 10.1002/mame.201200285.
7. I. Zembouai, M. Kaci, S. Bruzaud, A. Benhamida, Y.-M. Corre, Y. Grohens, *Polym. Test.* **2013**, *32*, 842, DOI: 10.1016/j.polymertesting.2013.04.004.

8. M. Zhang, N. L. Thomas, *Adv. Polym. Technol.* **2011**, *30*, 67, 10.1002/adv.20235.
9. B. Bittmann, R. Bouza, L. Barral, M. Castro-Lopez, S. Dopico-Garcia, *Polym. Comp.* **2015**, *36*, 2051, DOI: 10.1002/pc.23115.
10. Y. J. Phua, A. Pegoretti, T. M. Araujo, Z. A. M. Ishak, *J. Appl. Polym. Sci.* **2015**, *132*, DOI: 10.1002/app.42815.
11. K. Zhang, A. K. Mohanty, M. Misra, *ACS Appl. Mat. Interfaces* **2012**, *4*, 3091, DOI: 10.1021/am3004522.
12. J. Xu, B.-H. Guo, *Biotechnology Journal* **2010**, *5*, 1149, 10.1002/biot.201000136.
13. M. Salomez, M. George, P. Fabre, F. Touchaleaume, G. Cesar, A. Lajarrige, E. Gastaldi, *Polym. Degrad. Stab.* **2019**, *167*, 102, <https://doi.org/10.1016/j.polymdegradstab.2019.06.025>.
14. V. Tserki, P. Matzinos, E. Pavlidou, D. Vachliotis, C. Panayiotou, *Polym. Degrad. Stab.* **2006**, *91*, 367, DOI: 10.1016/j.polymdegradstab.2005.04.035.
15. M. Nofar, A. Tabatabaei, H. Sojoudiasli, C. B. Park, P. J. Carreau, M. C. Heuzey, M. R. Kamal, *Eur. Polym. J.* **2017**, *90*, 231, <https://doi.org/10.1016/j.eurpolymj.2017.03.031>.
16. V. Ojijo, S. Sinha Ray, R. Sadiku, *ACS Appl. Mat. Interfaces* **2012**, *4*, 6690, DOI: 10.1021/am301842e.
17. Y.-M. Corre, S. Bruzaud, J.-L. Audic, Y. Grohens, *Polym. Test.* **2012**, *31*, 226, <http://dx.doi.org/10.1016/j.polymertesting.2011.11.002>.
18. S. Charlon, N. Follain, E. Dargent, J. Soulestin, M. Sclavons, S. Marais, *J. Chem. Phys C* **2016**, *120*, 13234, DOI: 10.1021/acs.jpcc.6b00339.
19. S. Weinmann, C. Bonten, *Polym. Eng. Sci.* **2019**, *59*, 1057, DOI: 10.1002/pen.25075.
20. H. P. Grace†, *Chem. Eng. Comm.* **1982**, *14*, 225, DOI: 10.1080/00986448208911047.
21. L. A. Utracki, *J. Rheol.* **1991**, *35*, 1615, DOI: 10.1122/1.550248.
22. T. Debuissy, E. Pollet, L. Avérous, *Eur. Polym. J.* **2017**, *87*, 84, <https://doi.org/10.1016/j.eurpolymj.2016.12.012>.
23. T. Liu, Z. Mo, S. Wang, H. Zhang, *Polym. Eng. Sci.* **1997**, *37*, 568, <https://doi.org/10.1002/pen.11700>.
24. M. Avrami, *J. Chem. Phys.* **1941**, *9*, DOI: 177, 10.1063/1.1750872.
25. M. Avrami, *J. Chem. Phys.* **1940**, *8*, 212, DOI: 10.1063/1.1750631.
26. M. Avrami, *J. Chem. Phys.* **1939**, *7*, 1103, DOI: 10.1063/1.1750380.
27. Y. S. Chun, W. N. Kim, *Polymer* **2000**, *41*, 2305, DOI: 10.1016/s0032-3861(99)00534-0.
28. Y. S. Chun, W. N. Kim, *J. Appl. Polym. Sci.* **2000**, *77*, 673, [https://doi.org/10.1002/\(SICI\)1097-4628\(20000718\)77:3%3C673::AID-APP22%3E3.0.CO;2-1](https://doi.org/10.1002/(SICI)1097-4628(20000718)77:3%3C673::AID-APP22%3E3.0.CO;2-1).
29. A. Buzarovska, A. Grozdanov, *J. Mater. Sci.* **2009**, *44*, 1844, DOI:10.1007/s10853-008-3236-3.
30. N. Jiang, H. Abe, *J. Appl. Polym. Sci.* **2015**, *132*, 8, DOI: 10.1002/app.42548.
31. Z. B. Qiu, T. Ikehara, T. Nishi, *Polymer* **2003**, *44*, 7519, DOI:10.1016/j.polymer.2003.09.029.
32. H. Li, X. Lu, H. Yang, J. Hu, *J. Thermal Anal. Calorim.* **2015**, *122*, 817, DOI:10.1007/s10973-015-4824-5.
33. P. J. Barham, A. Keller, *J. Polym. Sci. Pt. B-Polym. Phys.* **1986**, *24*, 69, 10.1002/polb.1986.180240108.
34. A. El-Hadi, R. Schnabel, E. Straube, G. Müller, S. Henning, *Polym. Test.* **2002**, *21*, 665, [https://doi.org/10.1016/S0142-9418\(01\)00142-8](https://doi.org/10.1016/S0142-9418(01)00142-8).
35. T. Wan, J. Zhang, S. Liao, T. Du, *Polym. Eng. Sci.* **2015**, *55*, 966, <https://doi.org/10.1002/pen.23966>.
36. C. Y. Wan, E. L. Heeley, Y. T. Zhou, S. F. Wang, C. T. Cafolla, E. M. Crabb, D. J. Hughes, *Soft Matter* **2018**, *14*, 9175, DOI: 10.1039/c8sm01889h.

37. J. Kolarik, *Polym. Eng. Sci.* **1996**, *36*, 2518, DOI:10.1002/pen.10650.
38. P.-G. De Gennes, *J. Physique Lett.* **1976**, *37*, 1, DOI: 10.1051/jphyslet:019760037010100.
39. J. Kolařík, *Polymer* **1996**, *37*, 887, [https://doi.org/10.1016/0032-3861\(96\)87270-3](https://doi.org/10.1016/0032-3861(96)87270-3).